coatings

MDPI

Article

Quantum Chemical and Monte Carlo Simulation Studies on Inhibition Performance of Caffeine and Its Derivatives against Corrosion of Copper

Saprizal Hadisaputra [1,*], Agus Abhi Purwoko [1], Lalu Rudyat Telly Savalas [1], Niko Prasetyo [2], Emmy Yuanita [3] and Saprini Hamdiani [3,4]

1 Chemistry Education Division, University of Mataram, Jalan Majapahit 62, Mataram 83125, Indonesia; agus_ap@unram.ac.id (A.A.P.); telly@unram.ac.id (L.R.T.S.)
2 Austrian-Indonesian Centre for Computational Chemistry, FMIPA, Universitas Gadjah Mada, Sekip Utara, Yogyakarta 55281, Indonesia; nikop@ugm.ac.id
3 Department of Chemistry, University of Mataram, Jalan Majapahit 62, Mataram 83125, Indonesia; emmy_yuanita@unram.ac.id (E.Y.); saprini.h@unram.ac.id (S.H.)
4 Department of Applied Chemistry, Chaoyang University and Technology, Taichung 41349, Taiwan
* Correspondence: rizall@unram.ac.id; Tel.: +62-877-380-664-22

Received: 13 October 2020; Accepted: 3 November 2020; Published: 13 November 2020

Abstract: Performance tests on caffeine's corrosion inhibition properties and their derivatives against copper corrosion have been previously reported experimentally using gravimetric and electrochemical analyses. The test was able to measure the efficiency of their corrosion inhibition accurately. However, the caffeine and its derivatives' structure patterns and coating mechanisms when interacting with metals during copper corrosion inhibition have not been explained in detail by experimental studies. In the present study, the theoretical density functional study (DFT), ab initio MP2, and Monte Carlo simulation approaches explain the problem. The geometrical and quantum chemical parameters of inhibitors were compared under normal and protonated conditions in the gas and aqueous environments. Theoretical studies can accurately determine the molecule's geometrical parameters and successfully explain the quantum parameters of inhibitors. Molecular dynamics are applied to study the mechanism of interaction between inhibitors and metal surfaces in an explicit water molecule environment. The energy absorption of caffeine and its derivatives on metal surfaces was linear, with quantum parameters calculated from the density functional theory and an ab initio approach. Furthermore, these theoretical study results align with the previously reported experimental studies published by de Souza et al. The inhibition efficiency ranking of studied molecules preventing copper corrosion was caffeine > theobromine > theophylline. This theoretical approach is expected to bridge the gap in designing effective corrosion inhibitors.

Keywords: density functional theory; ab initio; monte carlo; caffeine; copper; corrosion inhibition

1. Introduction

Corrosion is an electrochemical process in metals that damages metal structures. This process is usually triggered by corrosive environments such as hydrochloric acid and nitric acid. The corrosion process is challenging to overcome, and without prevention, corrosion will cause significant economic losses [1]. Therefore, research to find corrosion inhibitors that are environmentally friendly, economical, and of high efficiency, is still being carried out intensively. Organic compounds from natural products have a high potential to be developed as corrosion inhibitors. This compound was chosen as a corrosion inhibitor because it meets the criteria of high efficiency, economical, environmentally friendly, and non-toxic, and it does not cause harmful pollutants [2–4].

Many experimental studies on the efficiency of corrosion inhibition of natural product compounds have been carried out [5–7]. For example, alkaloids obtained from natural product extraction have high potential as good corrosion inhibitors [8–10]. The main factors that play a role in inhibiting corrosion are electrostatic interactions, Π electron donors, and heteroatom groups on inhibitor molecules [11]. Heterocyclic benzene and heteroatom groups such as oxygen and nitrogen in the alkaloid structure play a role in electron donors, electrostatic interactions, and electron donor acceptors in their interactions with metal surfaces. These factors will be utilized by the inhibitor to be firmly attached to the metal surface and form a thin layer that will inhibit the rate of corrosion [12].

Caffeine is an alkaloid extracted from natural products that have been tested for its corrosion inhibition efficiency [13–15]. Fallavena et al. examined caffeine's ability to inhibit corrosion on copper surfaces in a solution of potassium nitrate using electrochemical techniques. The experimental results show that caffeine can inhibit corrosion by decreasing the corrosion rate in copper [16]. Combining complex caffeine-Zn^{2+} systems has also been studied to optimize caffeine's corrosion inhibition efficiency against copper corrosion. The complex is capable of forming caffeine-Zn^{2+} film complex formation on metal surfaces [17]. Other studies also show that caffeine can coat the carbon steel surface in ethanol solvents to prevent corrosion [18]. Moreover, caffeine has also been tested to inhibit corrosion on the surface of the nickel. Ebadi et al. showed that caffeine was well adsorbed on nickel's surface with an inhibitory efficiency of 96.8% [19]. Furthermore, caffeine derivatives have been assessed for their ability to reduce corrosion in copper. de Souza et al. showed that caffeine effectively inhibited copper corrosion than theobromine and theophylline [20].

Accurate measurement of the corrosion inhibitor performance of a compound can be done experimentally. However, this technique has a limitation: the mechanism of inhibition by inhibitors on metal surfaces may not be explained in detail. The cost and time of research is expensive. For an instant, de Souza et al. experimentally showed that caffeine more effectively inhibited copper corrosion than theobromine and theophylline [20]. However, de Souza et al. have not explained why caffeine is more efficient at inhibiting corrosion than theobromine and theophylline. The detailed pattern and mechanism of interactions between caffeine, theobromine, theophylline, and copper surfaces are not well explained. Therefore, the theoretical study supported by computer hardware and software development is a bridge to overcome this gap. The density functional theory approaches [21–25], ab initio [26–28] can explain in detail about the distribution and transfer of electrons when inhibitors interact with metals. Furthermore, the Monte Carlo simulation can explain in detail the effect of orientation and structure on the performance of each inhibitor, including the mechanism of adsorption of inhibitor molecules on metal surfaces. The density functional theory approaches [21–25], ab initio [26–28], and molecular dynamics simulation can explain in detail the effect of orientation and structure on the performance of each inhibitor, including the mechanism of adsorption of inhibitor molecules on metal surfaces [29,30]. Kaya et al. [31,32] combined DFT calculations at various theoretical and dynamic molecular levels to predict iron corrosion inhibition performance by thiazole and piperidine derivatives. It was reported that the strength of the interaction between thiazole and the surface of Fe (110) is determined by the orientation of the molecule and its donor and electron-withdrawing groups [31,32]. The theoretical studies that have been carried out show compatibility with experimental studies. The current report focuses on examining caffeine's performance and its derivatives as a corrosion inhibitor on copper's surface theoretically by combining the density functional theory, ab initio, and Monte Carlo simulation simultaneously. This research will also present the coating mechanism of caffeine and its derivatives on the copper surface.

2. Materials and Methods

2.1. Quantum Chemical Calculations

Quantum chemical calculations are applied to predict the structure and electron distribution of caffeine, theobromine, theophylline, and their electron transfer to the copper surface. Density functional

theory is a very popular method for assessing the reactivity of molecules [33]. The ab initio method is also widely used because it has high accuracy [34]. In the quantum chemical calculation section, all calculations, including optimization of caffeine, theobromine, and theophylline, are carried out using the DFT and MP2 methods in a combination of 6-31G(d) and 6-311++G(d,p) basis sets. Geometry optimizations have been performed without any symmetry constraints. Optimized geometries are always verified as minimum energy potential surface by calculating the harmonic vibration frequencies. All quantum chemical calculations use the Gaussian 09 program [35]. Solvent effects are included using the polarized continuum model as implemented in the Gaussian code. The dielectric constant for the water solvent was taken as 78.4, and other solvents were used as in the Gaussian code. In employing polarized continuum models, the single-point calculations on gas-phase geometries are sufficient for energetics. The structure of re-optimization in the solvent's presence was found to have a minor influence on energetics [36,37]. Therefore, the single point approach has been employed in this study, minimizing computational costs without sacrificing much accuracy in solvation energies.

The quantum chemical parameters such as the energy of the highest occupied molecular orbital (EHOMO), the energy of the lowest unoccupied molecular orbital (ELUMO), the ionization potential (I), the electron affinity (A), the absolute electronegativity (χ), hardness (η), softness (σ), the fraction of electron transferred (ΔN), and the corrosion inhibitors (IE%) efficiencies were calculated. According to Koopman's theorem [38], ionization potential (I) and electron affinity (A), the electronegativity (χ), and global hardness (η) may be defined in terms of the EHOMO and the ELUMO. Ionization potential (I) is defined as the amount of energy required to remove an electron from a molecule [39]. It is related to the energy of the EHOMO through the Equation (1):

$$I = -EHOMO \quad (1)$$

Electron affinity (A) is defined as the energy released when a proton is added to a system [39]. It is related to ELUMO through the Equation (2):

$$A = -ELUMO \quad (2)$$

Electronegativity is the measure of the power of an atom or group of atoms to attract electrons towards itself [40]; it can be estimated by using the Equation (3):

$$\chi = \frac{I + A}{2} \quad (3)$$

Chemical hardness (η) measures an atom's resistance to a charge transfer [41]; it is estimated by using the Equation (4):

$$\eta = \frac{I - A}{2} \quad (4)$$

According to Pearson theory [42], the fraction of transferred electrons (ΔN) from the caffeine, theobromine and theophylline to the copper atom can be calculated Equation (5):

$$\Delta N = \frac{\chi\,Cu - \chi\,Inh}{2(\eta Cu + \eta Inh)} \quad (5)$$

where χCu and χinh denote the absolute electronegativity of copper and inhibitor molecule respectively, ηCu and ηinh denote the absolute hardness of copper and the inhibitor molecule, respectively. To calculate the fraction of electrons transferred, the theoretical value for bulk iron's electronegativity was used χCu = 4.43 eV [43] and a global hardness of ηCu = 0 by assuming that for a metallic bulk I = A [44].

The Fukui indices for the nucleophilic and electrophilic sites (f^+ and f^-) are expressed [45] via Equations (6) and (7).

$$f^+ = qN + 1 - qN \text{ (nucleophilic attack)} \quad (6)$$

$$f^- = qN - qN - 1 \text{ (electrophilic attack)} \quad (7)$$

According to Koopman's theorem [38], ionization potential (I) and electron affinity (A), the electronegativity (χ), and global hardness (η) may be defined in terms of the EHOMO and the ELUMO. Ionization potential (I) is defined as the amount of energy required to remove an electron from a molecule [39]. It is related to the EHOMO through the Equation (1).

2.2. Monte Carlo Simulations

The Monte Carlo simulation is very popular for investigating the interaction between the molecule inhibitor and the concerned metal surface [45–47]. The Monte Carlo simulation can explain a key element in the corrosion problem: the adsorption phenomenon. The most stable adsorption sites on metal surfaces with low energy. The Monte Carlo metropolis simulation methodology is used in molecular dynamics simulations performed using the adsorption locator and the Forcite code implemented in Material Studio 7.0 software [48,49]. The lowest conformational energy search is performed by adopting a Monte Carlo search of interactions between inhibitor molecules and clean copper surfaces in water. The COMPASS force field is used to optimize all the studied molecular structures. The advantages of the COMPASS force field are the ab initio force fields that allow accurate and simultaneous gas-phase predictions and condensation properties. Those properties, including structural, conformational, vibration and state equations, cohesive energy, interaction energy for a variety of organic metal molecules, metal oxides, and metal halides, use a variety of solid properties: the structure of cell units, lattice energy, and even polymers. The first step in this computational study is to optimize the geometry of the inhibitor molecule: caffeine, theobromine, and theophylline, which will adsorb next on the copper surface with minimized energy. For this purpose, the Forcite calculation was performed with the fine calculation quality using the COMPASS forcefield. Once the caffeine, theobromine, and theophylline have been optimized with the COMPASS forcefield, we simulate those corrosion inhibitors by loading with a copper surface, considering the solvent effect. The objective of this computational study is to find the low-energy adsorption sites to investigate the preferential adsorption of caffeine, theobromine, and theophylline on Cu(1 1 1) surface and to find a relationship between the effect of their molecular structure and their inhibition efficiency. The simulation protocol details follow the simulation steps that have been carried out previously [50] with the crystal surface of Cu(111) in the simulation box (20.447831 Å × 20.447831 Å × 40.43474 Å) with periodic boundary conditions to simulate the representative part of the interface without arbitrary boundary effects. The Cu plane (111) was further enlarged to supercell (8 × 8). After that, a vacuum slab with a 3.0 nm thickness was built on the Cu plane (111). The three caffeine, theobromine, and theophylline corrosion inhibitors, along with 100 water molecules, are used for simulations in each case. Water is essential in simulations because it plays a vital role in corrosion in the natural environment.

3. Results and Discussion

The theoretical study can be very close to wet laboratory experiment data, or it can also be incompatible. As a consequence of using quantum mechanical methods in theoretical calculations, it is necessary to validate the theoretical approach by comparing experimental data [51]. For this purpose, we have tested the compatibility of the 6-311++G (d,p) method and basis set options with the studied system (Figure 1). Comparisons were made between theoretical study results with the crystal structures of the three previously published inhibitor molecules: caffeine [52], theobromine [53], and theophylline [54]. It was used to test the accuracy of theoretical calculations in terms of molecular geometry parameters. The experimental results' geometry parameters compared with the theoretical calculation using the DFT/6-311++G (d,p) method are depicted in Table 1. Table 1 shows the linear

correlation between experimental X-ray and theoretical data. The difference in bond lengths and bonding angles of the X-ray structure of experiments and theoretical studies for the three compounds is 0.03 Å and 0.65°, respectively. The small difference between theoretical and experimental shows that the level of methods and the basis of the theoretical set of studies can be applied to the system being studied.

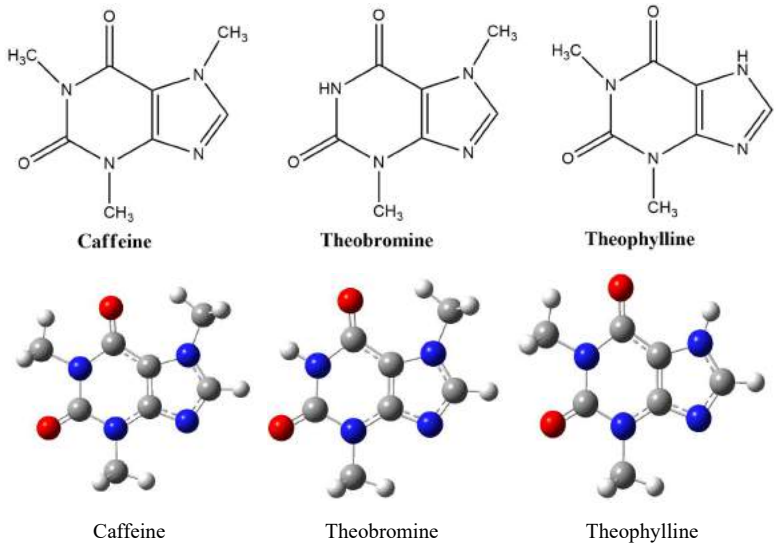

Figure 1. Optimized geometry of caffeine, theobromine, theophylline at B3LYP/6-311++G(dp) level of theory.

Table 1. Structural parameters of the optimized geometry of caffeine, theobromine, theophylline at B3LYP/6-311++G(d,p) level of theory.

Bond	Caffeine		Theophyllien						Theobromine					
	Exp	B3LYP	Bond	Exp	B3LYP	Bond Angle	Exp	B3LYP	Bond Angle	Exp	B3LYP	Bond Angle	Exp	B3LYP
N1-C2	1.42	14.083	N1-C2	1.41	1.408	C2-N1-C6	126.6	126.821	N1-C2	1.381	1.401	C2-N1-C6	1291	130.007
N1-C6	1.36	14.165	N1-C6	1.41	1.417	C2-N1-C10	117.1	115.160	N1-C6	1.397	1.407	C2-N1-H1	116.7	114.059
N1-C10	1.48	14.665	N1-C10	1.48	1.466	C6-N1-C10	116.3	118.018	N1-H1	0.85	1.013	C6-N1-H1	114.2	115.933
C2-N3	1.35	13.907	C2-N3	1.36	1.393	N1-C2-N3	117.4	117.267	C2-N3	1.377	1.390	N1-C2-N3	116.4	115.304
C2-O11	1.19	12.226	C2-O11	1.22	1.222	N1-C2-O11	120.2	121.383	C2-O11	1.231	1.220	N1-C2-O11	121.5	121.926
N3-C4	1.42	13.761	N3-C4	1.38	1.375	N3-C2-O11	122.4	121.349	N3-C4	1.377	1.380	N3-C2-O11	112.1	122.768
N3-C12	1.50	14.622	N3-C12	1.46	1.462	C2-N3-C4	119.7	119.660	N3-C12	1.473	1.462	C2-N3-C4	118.9	119.647
C4-C5	1.32	13.821	C4-C5	1.34	1.378	C2-N3-C12	120.1	118.109	C4-C5	1.364	1.385	C2-N3-C12	119.2	118.221
C4-N9	1.31	13.596	C4-N9	1.35	1.363	C4-N3-C12	120.2	122.229	C4-N9	1.363	1.359	C4-N3-C12	121.8	122.131
C5-C6	1.44	14.345	C5-C6	1.43	1.432	C4-C5-N7	105.4	104.763	C5-C6	1.426	1.436	N3-C4-C5	122.4	122.212
C5-N7	1.41	13.892	C5-N7	1.38	1.382	C6-C5-N7	129.8	130.877	C5-N7	1.388	1.387	N3-C4-N9	124.9	126.188
C6-O13	1.26	12.300	C6-O13	1.21	1.226	N1-C6-C5	110.1	110.772	C6-O13	1.225	1.227	C5-C4-N9	112.7	111.598
N7-C8	1.32	13.558	N7-C8	1.32	1.357	N1-C6-O13	122.0	123.169	N7-C8	1.343	1.355	C4-C5-C6	122.9	123.104
N7-C14	1.47	14.619	N7-H7	0.90	1.010	C5-C6-O13	127.9	126.057	N7-C10	1.469	1.462	C4-C5-N7	105.1	105.144
C8-N9	1.34	13.300	C8-N9	1.31	1.327	C5-N7-C8	105.7	128.262	C8-N9	1.339	1.330	C6-C5-N7	132.0	131.750
-	-	-	C8-H8	1.02	1.081	C5-N7-H7	128.0	106.529	C8-H8	1.03	1.082	N1-C6-C5	110.3	109.722

Electron transfer between molecules can be studied by showing the conditions of molecular orbitals. The interaction between the highest occupied molecular orbitals (HOMO) and the lowest unoccupied molecular orbitals (LUMO) is the cause of electron transfer between molecules [39]. Electron transfer can be measured using energy values from orbitals. HOMO energy (E_{HOMO}) indicates a molecule's nature to donate its electrons, while LUMO energy (E_{LUMO}) indicates the nature of a molecule to receive electrons. The greater the E_{HOMO} or, the smaller E_{LUMO}, the greater the electron donor so that the stronger an organic molecule is attached to the metal. As a consequence, these organic molecules will have high corrosion inhibition efficiency. Tables 2–5 show the quantum chemical parameters for caffeine, theobromine, and theophylline, which were calculated using DFT and MP2 at

theoretical levels 6-31G(d) and 6-311++G(d,p). All quantum chemical parameter data in Tables 2–5 were calculated as given by Equations (1)–(5). Tables 2–5 show that the increase in E_{HOMO} value is caffeine > theobromine > theophylline. The E_{HOMO} calculated using MP2/6-31G(d) for caffeine is −8.5411 eV, while the E_{HOMO} for theophylline is the lowest, −8.6866 eV. These predictions from E_{HOMO} suggest that caffeine will have the highest corrosion inhibition efficiency (IE%) compared to the other two compounds. This theoretical result is following an experimental study conducted previously by de Souza et al. They explained that the order of efficiency of corrosion inhibition of copper metal in acidic medium was caffeine > theobromine > theophylline [20]. The distribution of electrons in molecular orbitals on caffeine, theobromine, and theophylline is visualized in Figure 2. The difference in electron distribution in the three compounds is apparent where caffeine has a wider electron distribution. It strengthens the predicted EHOMO-related sequence of enhancing inhibitor performance.

Table 2. The calculated quantum chemical parameters of neutral caffeine, theobromine, and theophylline in the gas phase at a different level of theory. (All values are in eV).

Compound	E_{HOMO}	E_{LUMO}	ΔE	*I*	*A*	χ	η	ΔN
Caffeine								
B3LYP/6-31G(d)	−5.9576	−0.8781	−5.0795	5.9576	0.8781	3.4178	2.5397	0.2090
B3LYP/6-311++G(dp)	−6.3310	−1.3785	−4.9524	6.3310	1.3785	3.8547	2.4762	0.1262
MP2/6-31G(d)	−8.5411	2.9102	−11.4513	8.5411 (8.31) [a]	−2.9102	2.8154	5.7256	0.1453
MP2/6-311++Gdp	−8.7068	0.8095	−9.5163	8.7068	−0.8095	3.9486	4.7581	0.0558
Theobromine								
B3LYP/6-31G(d)	−6.0401	−0.9529	−5.0871	6.0401	0.9529	3.4965	2.5435	0.1933
B3LYP/6−311++G(dp)	−6.4455	−1.4966	−4.9489	6.4455	1.4966	3.9710	2.4744	0.1028
MP2/6-31G(d)	−8.6401	2.8389	−11.4799	8.6401 (8.31) [b]	−2.8389	2.9005	5.7395	0.1375
MP2/6-311++G(dp)	−8.8284	0.7760	−9.6045	8.8284	−0.7760	4.0261	4.8022	0.0472
Theophylline								
B3LYP/6-31G(d)	−6.0735	−0.9208	−5.1527	6.0735	0.9208	3.4972	2.5763	0.1907
B3LYP/6−311++G(dp)	−6.4828	−1.4362	−5.0466	6.4828	1.4362	3.9595	2.5233	0.1031
MP2/6-31G(d)	−8.6866	2.8879	−11.5741	8.6866 (8.30) [b]	−2.8879	2.8993	5.7873	0.1365
MP2/6-311++G(dp)	−8.8779	0.7436	−9.62169	8.8779	−0.7436	4.0671	4.8108	0.0429

[a] [55], [b] [56].

Table 3. The calculated quantum chemical parameters of protonated caffeine, theobromine, and theophylline in the gas phase at different levels of theory. (All values are in eV).

Compound	E_{HOMO}	E_{LUMO}	ΔE	*I*	*A*	χ	η	ΔN
Protonated								
B3LYP/6-31G(d)	−10.6562	−5.6330	−5.0232	10.6562	5.6330	8.1446	2.5116	−0.7295
B3LYP/6-311++G(dp)	−10.8929	−5.9524	−4.9405	10.8929	5.9524	8.4227	2.4702	−0.7980
MP2/6-31G(d)	−13.2837	−1.6865	−11.597	13.2837	1.6865	7.4851	5.7986	−0.2591
MP2/6-311++Gdp	−13.3526	−2.4631	−10.889	13.3526	2.4631	7.9079	5.4447	−0.3147
Protonated								
B3LYP/6-31G(d)	−10.7909	−5.8177	−4.9731	10.7909	5.8177	8.3043	2.4865	−0.7690
B3LYP/6-311++G(dp)	−11.0442	−6.1633	−4.8809	11.0442	6.1633	8.6038	2.4404	−0.8448
MP2/6-31G(d)	−13.4056	−1.8754	−11.5302	13.4056	1.8754	7.6405	5.7651	−0.2741
MP2/6-311++Gdp	−13.4870	−2.5374	−10.9495	13.4870	2.5374	8.0122	5.4747	−0.3225
Protonated								
B3LYP/6-31G(d)	−10.8252	−5.9495	−4.8757	10.8252	5.9495	8.3873	2.4378	−0.8013
B3LYP/6-311++G(dp)	−11.0780	−6.2885	−4.7894	11.0780	6.2885	8.6832	2.3947	−0.8776
MP2/6-31G(d)	−13.4511	−2.0049	−11.4462	13.4511	2.0049	7.7280	5.7231	−0.2837
MP2/6-311++Gdp	−13.5325	−2.6169	−10.9155	13.5325	2.6169	8.0747	5.4577	−0.3293

Table 4. The calculated quantum chemical parameters of neutral caffeine, theobromine, and theophylline in the aqueous phase at a different level of theory. (All values are in eV).

Compound	E_{HOMO}	E_{LUMO}	ΔE	*I*	*A*	χ	η	ΔN
Caffeine								
B3LYP/6-31G(d)	−5.9941	−0.8835	−5.1105	5.9941	0.8835	3.4388	2.5552	0.6968
B3LYP/6-311++G(dp)	−6.3421	−1.3426	−4.9995	6.3421	1.3426	3.8423	2.4997	0.6315
MP2/6-31G(d)	−8.5375	2.9459	−11.4833	8.5375	−2.9459	2.7958	5.7417	0.3661
MP2/6-311++Gdp	−8.6842	1.0930	−9.7773	8.6842	−1.0930	3.7955	4.8886	0.3277
Theobromine								
B3LYP/6-31G(d)	−6.0379	−0.9183	−5.1195	6.0379	0.9183	3.4781	2.5597	0.6879
B3LYP/6-311++G(dp)	−6.4118	−1.4188	−4.9930	6.4118	1.4188	3.9153	2.4965	0.6178
MP2/6-31G(d)	−8.5922	2.9165	−11.5087	8.5922	−2.9165	2.8378	5.7543	0.3616
MP2/6-311++G(dp)	−8.7574	1.1292	−9.8867	8.7574	−1.1292	3.8140	4.9433	0.3222
Theophylline								
B3LYP/6-31G(d)	−6.0675	−0.8851	−5.1824	6.0675	0.8851	3.4763	2.5912	0.6799
B3LYP/6-311++G(dp)	−6.4466	−1.3681	−5.0784	6.4466	1.3681	3.9074	2.5392	0.6089
MP2/6-31G(d)	−8.6347	2.9616	−11.5964	8.6347	−2.9616	2.8365	5.7982	0.3593
MP2/6-311++G(dp)	−8.8037	1.0982	−9.9019	8.8037	−1.0982	3.8527	4.9509	0.3178

Table 5. The calculated quantum chemical parameters of protonated caffeine, theobromine, and theophylline in the aqueous phase at different theory levels. (All values are in eV).

Compound	E_{HOMO}	E_{LUMO}	ΔE	*I*	*A*	χ	η	ΔN
Protonated Caffeine								
B3LYP/6-31G(d)	−7.0355	−1.8084	−5.2270	7.0355	1.8084	4.4219	2.6135	0.4932
B3LYP/6-311++G(dp)	−7.2730	−2.1284	−5.1445	7.2730	2.1284	4.7007	2.5722	0.4469
MP2/6-31G(d)	−9.5890	2.2329	−11.8219	9.5890	−2.2329	3.6780	5.9109	0.2809
MP2/6-311++Gdp	−9.6586	0.9875	−10.6461	9.6586	−0.9875	4.3355	5.3230	0.2502
Protonated Theobromine								
B3LYP/6-31G(d)	−7.0736	−1.8784	−5.1952	7.0736	1.8784	4.4760	2.5976	0.4858
B3LYP/6-311++G(dp)	−7.3283	−2.2250	−5.1032	7.3283	2.2250	4.7766	2.5516	0.4356
MP2/6-31G(d)	−9.6192	2.1717	−11.7909	9.6192	−2.1717	3.7237	5.8954	0.2778
MP2/6-311++Gdp	−9.7005	1.0201	−10.7207	9.7005	−1.0201	4.3402	5.3603	0.2480
Protonated Theophylline								
B3LYP/6-31G(d)	−7.0785	−1.8990	−5.1794	7.0785	1.8990	4.4887	2.5897	0.4848
B3LYP/6-311++G(dp)	−7.3321	−2.2397	−5.0923	7.3321	2.2397	4.7859	2.5461	0.4347
MP2/6-31G(d)	−9.6306	2.1760	−11.8067	9.6306	−2.1760	3.7272	5.9033	0.2771
MP2/6-311++Gdp	−9.7106	0.9948	−10.7055	9.7106	−0.9948	4.3579	5.35275	0.2467

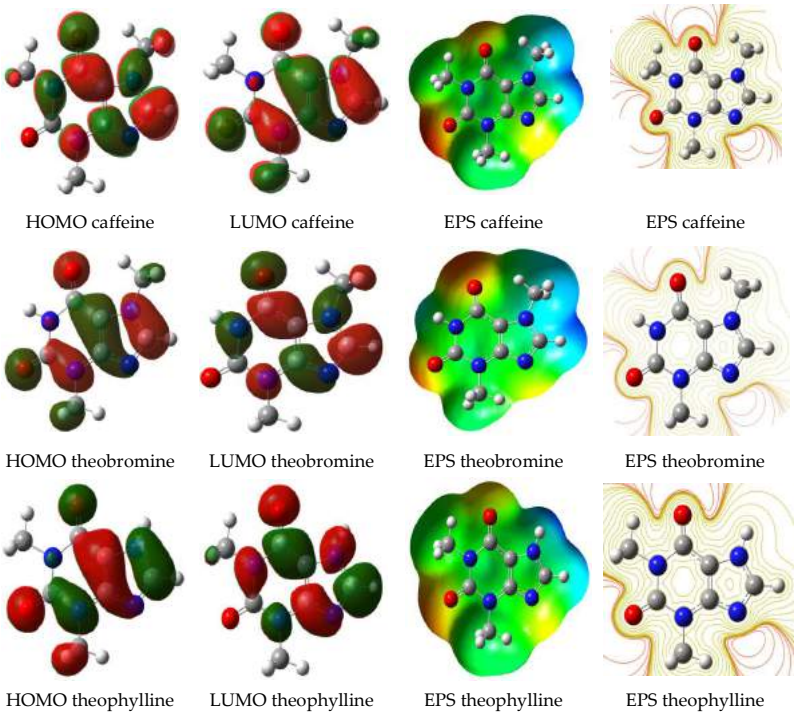

Figure 2. Visualization of highest occupied molecular orbitals–lowest unoccupied molecular orbitals (HOMO–LUMO) energies and electrostatic potential of caffeine and its derivatives.

Ionization potential (I) can be used to measure the reactivity of a molecule. A high ionization potential indicates that the molecule has high reactivity, while a low ionization potential value indicates the molecule has a low reactivity [39]. Tables 2–5 also show the pattern of increase in ionization potential, which follows the pattern of increase of EHOMO. The potential ionization value of caffeine calculated using MP2/6-31G (d) is 8.5411 eV, and it is lower than the potential ionization value of theobromine and theophylline. Based on this ionization potential, it can be predicted that caffeine has a higher corrosion inhibition efficiency (IE%) than theobromine and theophylline. This potential ionization value can also be used to test the accuracy of the theoretical calculation methods. The potential ionization value measured using DFT/B3LYP is far below the standard experimental value [55,56]. For example, experimentally, the value of caffeine's ionization potential is 8.31 eV, while DFT/B3LYP/6-311++G(d,p) gives a value of 6.3310 eV. The potential ionization value of DFT/B3LYP is 2 eV lower than the experimental results. It shows the weakness of DFT, which failed to imitate the energy of the experimental results. A similar finding was found by previous researchers [57–59], although DFT was successful in mimicking the results of the structural parameters, as seen in Table 1. We, therefore, recommend that DFT/B3LYP not be used to measure the energy of a quantum parameter of a molecule.

Small electronegativity values cause molecules to easily reach electron equilibrium so that the molecules get more reactive. In contrast, high electronegativity values show the opposite [40]. Tables 2–5 show how electronegativity increases are caffeine < theobromine < theophylline. The electronegativity value of caffeine that calculated using MP2/6-311++G(d,p) is the lowest (3.94 eV) compared to the electronegativity values for theobromine, and theophylline, which are 4.0261 and 4.0671 eV, respectively. Based on electronegativity data, it is predicted that caffeine has a higher corrosion inhibition efficiency (IE%) than theobromine and theophylline. Electronegativity obtained in theoretical calculations has a linear relationship with experimental studies from de Sousa et al. [20].

Tables 2–5 show that electron transfer also affects the corrosion inhibition efficiency of caffeine and its derivatives. The fraction of electrons (ΔN) quantifies the transfer of electrons from molecule to metal if $\Delta N > 0$, and from metal to molecule if $\Delta N < 0$ [60]. In general, the efficiency of corrosion inhibition increases as the value of the electron transfer increases, because the more electrons are transferred to the iron surface, the more electrons will coat the iron surface, so that the corrosion process can be inhibited [41]. The order of magnitude of the electron transfer for the three compounds to copper is caffeine > theobromine > theophylline. These results apply to all conditions in both the gas and solution phases, as well as for normal and protonated molecular conditions.

The local reactivity of caffeine, theobromine, and theophylline can be studied by observing the Fukui indices of each of their atoms. The Fukui indices provide more comprehensive information of the reactivity of the molecules under probe. In general, the numerical representation of the Fukui indices is the highest f^- the site indication for electrophilic attack or molecule receive electron, whereas the highest f^+ denotes the site for nucleophilic attack or when the molecule donates electrons [61,62].

The local reactivity of a molecule is analyzed using condensed Fukui indices as depicted in Table 6. For nucleophilic attack the most reactive sites of caffeine are O15, O16, and N24 atoms which are indicating the propensity to donate electrons to vacant molecular orbitals on the Fe (110) surface to form a coordinate bond, and the most reactive site for electrophilic attack is C17. The local softness indices also explain the comparison between reactivity of similar atoms of each part of different molecules. This result is linear with the calculation of HOMO density. For theobromine, the most nucleophilic sites are O11, O12, and N20 atoms, and the most electrophilic site is the C14 atom. For theophylline, the most nucleophilic sites are O11, O12, and N16 atoms, the most electrophilic site is the C13 atom. The electrophilic attack corresponds to the sites that most likely cause the molecule to accept electrons from the Fe (110) surface in the form of a back donation. This result corresponds to the LUMO energy values of caffeine, theobromine and theophylline.

Table 6. Calculated Mulliken atomic charge distribution and Fukui indices for caffeine, theobromine, and theophylline in condensed phase at the B3LYP/6-311++G(dp) level.

Caffein	**N−1**	**N**	**N+1**	$\mathbf{f^+}$	$\mathbf{f^-}$
C1	0.162586	0.155782	0.158459	0.002677	−0.006804
C2	−0.089031	−0.148159	−0.161602	−0.013443	−0.059128
C3	0.376028	0.469948	0.603219	0.133271	0.093920
C4	−0.446803	−0.411679	−0.451646	−0.039967	0.035124
N5	−0.120690	−0.102655	−0.032743	0.069912	0.018035
N6	−0.334752	−0.256422	−0.160822	0.095600	0.078330
C7	−0.194505	−0.206969	−0.216473	−0.009504	−0.012464
C8	−0.268936	−0.270889	−0.284398	−0.013509	−0.001953
H9	0.167456	0.195631	0.215417	0.019786	0.028175
H10	0.167444	0.195728	0.215478	0.019750	0.028284
H11	0.182352	0.195429	0.208032	0.012603	0.013077
H12	0.170662	0.182777	0.209048	0.026271	0.012115
H13	0.179276	0.198429	0.239475	0.041046	0.019153
H14	0.178993	0.198039	0.238854	0.040815	0.019046
O15	−0.470802	−0.410286	−0.273299	0.136987	0.060516
O16	−0.542781	−0.382377	−0.263297	0.119080	0.160404
C17	−0.042468	0.256205	0.346290	0.090085	0.298673
H18	0.191120	0.255362	0.312937	0.057575	0.064242
C19	−0.298899	−0.337688	−0.335998	0.001690	−0.038789
H20	0.138713	0.190666	0.219476	0.028810	0.051953
H21	0.198913	0.209085	0.221788	0.012703	0.010172
H22	0.139729	0.194213	0.223975	0.029762	0.054484
N23	−0.240805	−0.208855	−0.179672	0.029183	0.031950
N24	−0.202799	−0.161314	−0.052499	0.108815	0.041485
Theobromine	**−1**	**0**	**1**	$\mathbf{f^+}$	$\mathbf{f^-}$
C1	0.373874	0.374038	0.379773	0.005735	0.000164
C2	0.018911	−0.010603	−0.007031	0.003572	−0.029514
C3	−0.023784	0.077196	0.199807	0.122611	0.100980
C4	−0.103393	−0.073697	−0.101482	−0.027785	0.029696
N5	−0.100676	−0.086996	−0.017762	0.069234	0.013680
N6	−0.348486	−0.271648	−0.178983	0.092665	0.076838
C7	−0.299243	−0.301030	−0.312570	−0.011540	−0.001787
H8	0.167920	0.179710	0.205525	0.025815	0.011790
H9	0.178711	0.197757	0.237973	0.040216	0.019046
H10	0.178561	0.197558	0.237676	0.040118	0.018997
O11	−0.479782	−0.419618	−0.280301	0.139317	0.060164
O12	−0.576362	−0.400980	−0.276690	0.124290	0.175382
C13	−0.049400	0.223986	0.308130	0.084144	0.273386
H14	0.192142	0.255051	0.312138	0.057087	0.062909
C15	−0.310541	−0.345573	−0.343497	0.002076	−0.035032
H16	0.144336	0.194271	0.223403	0.029132	0.049935
H17	0.194748	0.204244	0.216713	0.012469	0.009496
H18	0.144840	0.195562	0.225038	0.029476	0.050722
N19	−0.468999	−0.430532	−0.409691	0.020841	0.038467
N20	−0.196793	−0.159632	−0.051456	0.108176	0.037161
H21	0.363416	0.400936	0.433287	0.032351	0.037520

Table 6. *Cont.*

Theophylline	−1	0	1	f^+	f^-
C1	0.175358	0.167927	0.169995	0.002068	−0.007431
C2	−0.324537	−0.373043	−0.413192	−0.040149	−0.048506
C3	0.472094	0.544694	0.696139	0.151445	0.072600
C4	−0.323918	−0.264517	−0.285707	−0.021190	0.059401
N5	−0.313234	−0.259961	−0.184856	0.075105	0.053273
N6	−0.343520	−0.256613	−0.162417	0.094196	0.086907
C7	−0.292243	−0.291210	−0.305278	−0.014068	0.001033
H8	0.163387	0.176023	0.203266	0.027243	0.012636
H9	0.181507	0.201215	0.243740	0.042525	0.019708
H10	0.181551	0.201278	0.243833	0.042555	0.019727
O11	−0.470998	−0.407345	−0.266334	0.141011	0.063653
O12	−0.578086	−0.399884	−0.271699	0.128185	0.178202
C13	0.036256	0.275613	0.363617	0.088004	0.239357
H14	0.196826	0.262887	0.317711	0.054824	0.066061
N15	−0.233768	−0.196546	−0.165706	0.030840	0.037222
N16	−0.193781	−0.151441	−0.037230	0.114211	0.042340
C17	−0.182087	−0.194383	−0.204253	−0.009870	−0.012296
H18	0.186109	0.200068	0.213343	0.013275	0.013959
H19	0.168038	0.197461	0.217926	0.020465	0.029423
H20	0.168028	0.197441	0.217894	0.020453	0.029413
H21	0.327017	0.370337	0.409207	0.038870	0.043320

The Monte Carlo Metropolis simulation is performed to find a possible position on the interaction between the inhibitor and the copper surface in aqueous solution. Figure 3 shows the most stable low energy adsorption configuration of the inhibitor in the Cu (111)/100H_2O system using a Monte Carlo simulation. The detailed analysis results on the shortest length of the active side bond of the inhibitor with copper are less than 3.50 A, which indicates the formation of a strong adhered layer between the inhibitor and the copper surface [63,64]. This layer coats the copper surface and prevents copper from being attacked by aggressive solutions. This strong layer bond also suggests the transfer of electron density from the inhibitor's active side to the d-orbitals of copper. This electron transfer causes strong interactions between the inhibitor and copper so that it can inhibit the rate of corrosion. Furthermore, van der Waals interactions are also involved in the adsorption of inhibitors with Cu surfaces. It is evident from observations with a bond distance above 3.50 A. Table 7 shows the adsorption energy for the most stable configurations for Cu(111)/Caffeine/100H_2O, Cu(111)/Theophylline/100H_2O, and Cu(111)/Theobromine/100H_2O systems. Table 7 also shows the adsorption energy of water. In all cases, the adsorption inhibitors' energy was much higher than water molecules (Table 7). It shows the possibility of gradual replacement of water molecules from the copper surface, which results in the formation of a stable layer that can protect the copper from aqueous corrosion. It can be seen from Table 6 that the energy of adsorption inhibitors on the iron surface in the presence of water decreases in the following sequence caffeine > theobromine > theophylline. This sequence is in accordance with an experimental study of caffeine, theobromine, and theophylline, which was carried out previously by de Souza et al. [20]. Caffeine has the best inhibitory ability while theophylline ranks lowest. The adsorption energy distribution of the inhibitors and water is depicted in Figure 4. It explains why caffeine is able to form a more stable layer on the copper surface than the other two inhibitors. Adsorption energy distribution in caffeine and water is separated from each other. In contrast, at some energy points of theobromine and theophylline adsorption energy distribution are almost the same as the adsorption energy distribution of water, so they form a weaker layer because, at some energy point, water is able to compete with them. Figures 5 and 6 show the correlation of the adsorption energy and quantum parameters of neutral and protonated inhibitors on copper surfaces. The Pearson correlation in Figures 5 and 6 indicates a linear correlation between energy adsorption and quantum parameters, especially EHOMO and ΔN. Still, it is not followed by electronegativity χ and hardness η. This shows

that EHOMO and ΔN play an essential role in the inhibitor's adsorption on the copper surface. It is generally recognized that the primary mechanism of interaction of corrosion inhibitors with copper is by adsorption. So, the adsorption energy can give us a direct tool for ranking inhibitory molecules. High negative adsorption energy indicates the system with the most stable and strong adsorption [64].

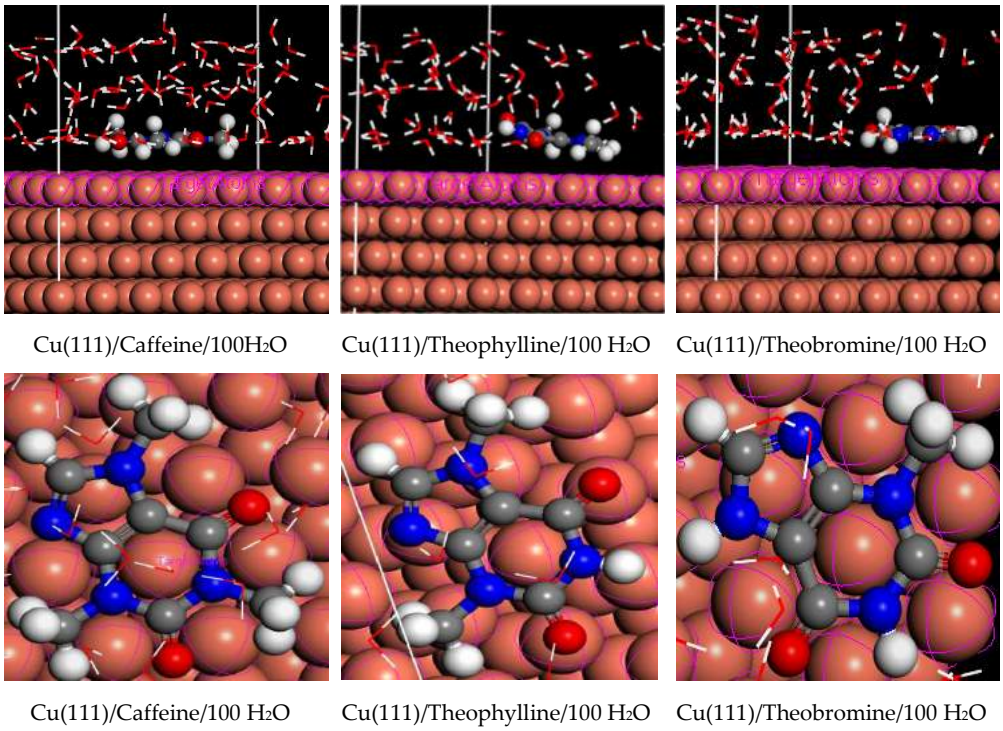

Figure 3. Top and side views of the most stable low energy configuration for the adsorption for Cu(111)/Caffeine/100H_2O, Cu(111)/Theophylline/100H_2O, and Cu(111)/Theobromine/100H_2O systems.

Table 7. Adsorption Energy for the most stable configurations for Cu(111)/Caffeine/100H_2O, Cu(111)/Theophylline/100H_2O and Cu(111)/Theobromine/100H_2O systems (all values are in kcal/mol).

Systems	Adsorption Energy (Inhibitor)	Adsorption Energy (Water)
Neutral Inhibitor		
Cu(111)/Caffeine/100 H_2O	−101.0518559	−12.5945366
Cu(111)/Theophylline/100 H_2O	−94.78979214	−14.61287273
Cu(111)/Theobromine/100 H_2O	−88.07084059	−13.9784625
Protonated Inhibitor		
Cu(111)/Caffeine/100 H_2O	−110.66243318	−15.30417885
Cu(111)/Theophylline/100 H_2O	−102.11197491	−13.54857608
Cu(111)/Theobromine/100 H_2O	−97.13070946	−13.90897810

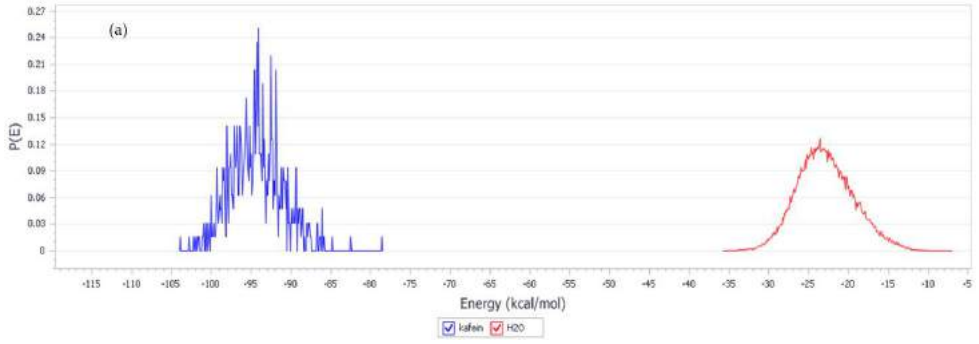

Figure 4. *Cont.*

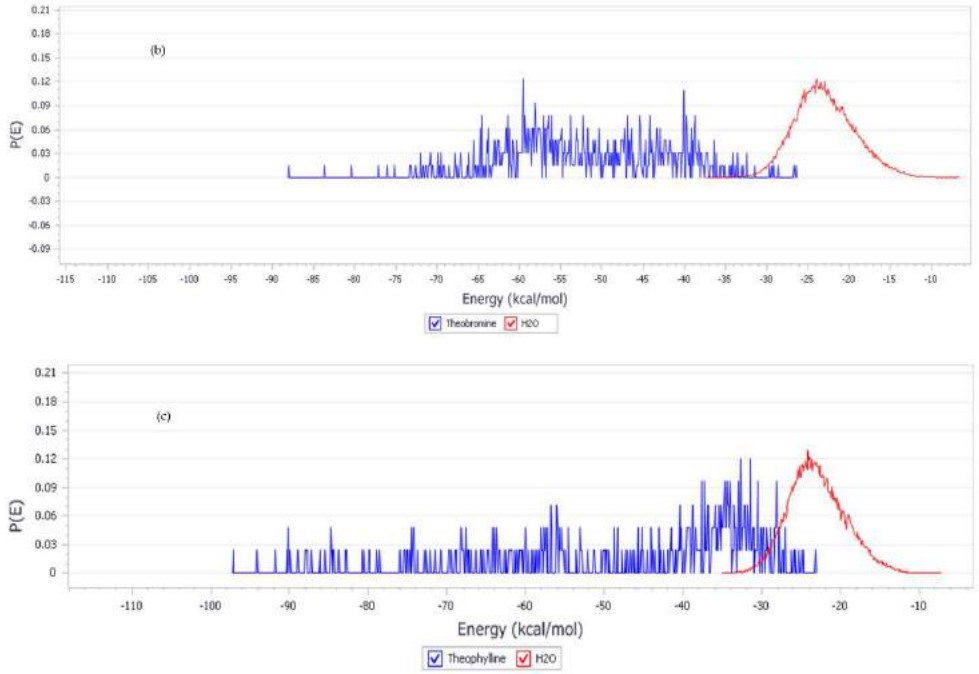

Figure 4. Adsorption energy distributions for (**a**) Cu(111)/Caffeine/100H_2O, (**b**) Cu(111)/ Theobromine /100H_2O, and (**c**) Cu(111)/ Theophylline /100H_2O systems.

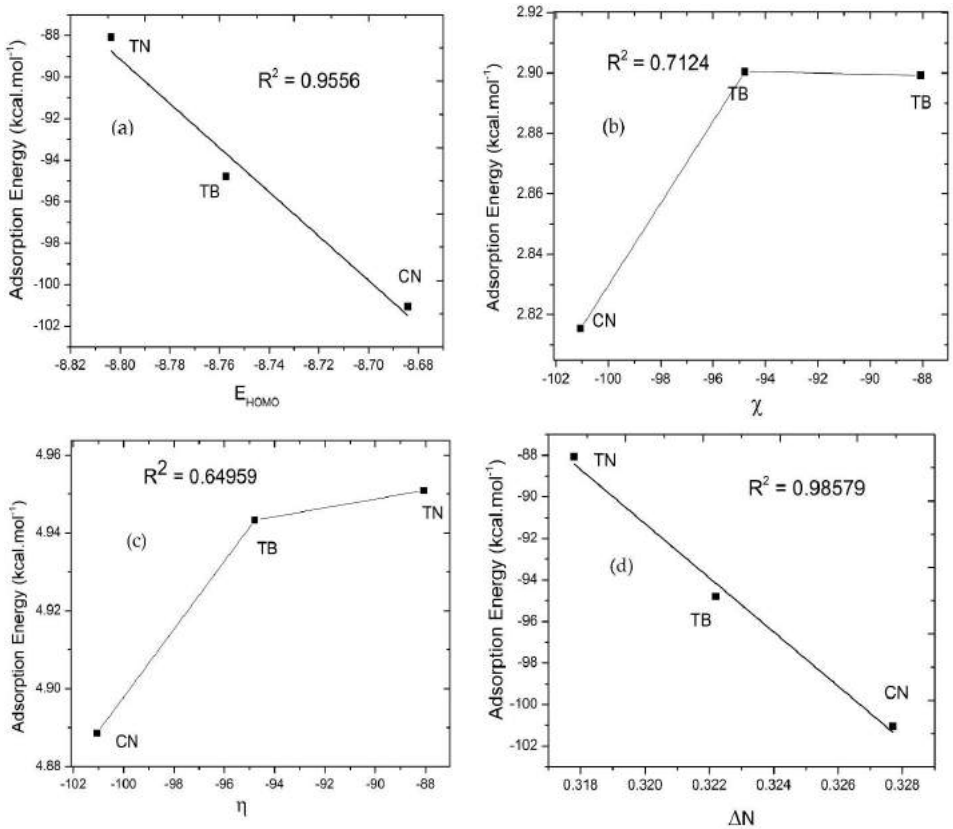

Figure 5. Correlation of the adsorption energy and quantum parameters such as EHOMO, electronegativity, hardness, and electron transfer of neutral inhibitors (caffeine (CN), theophylline (TP), and theobromine (TB)) in copper surface. (**a**) The correlation between the adsorption energy and EHOMO, (**b**) the adsorption energy and electronegativity, (**c**) the adsorption energy and hardness, (**d**) the adsorption energy and electron transfer.

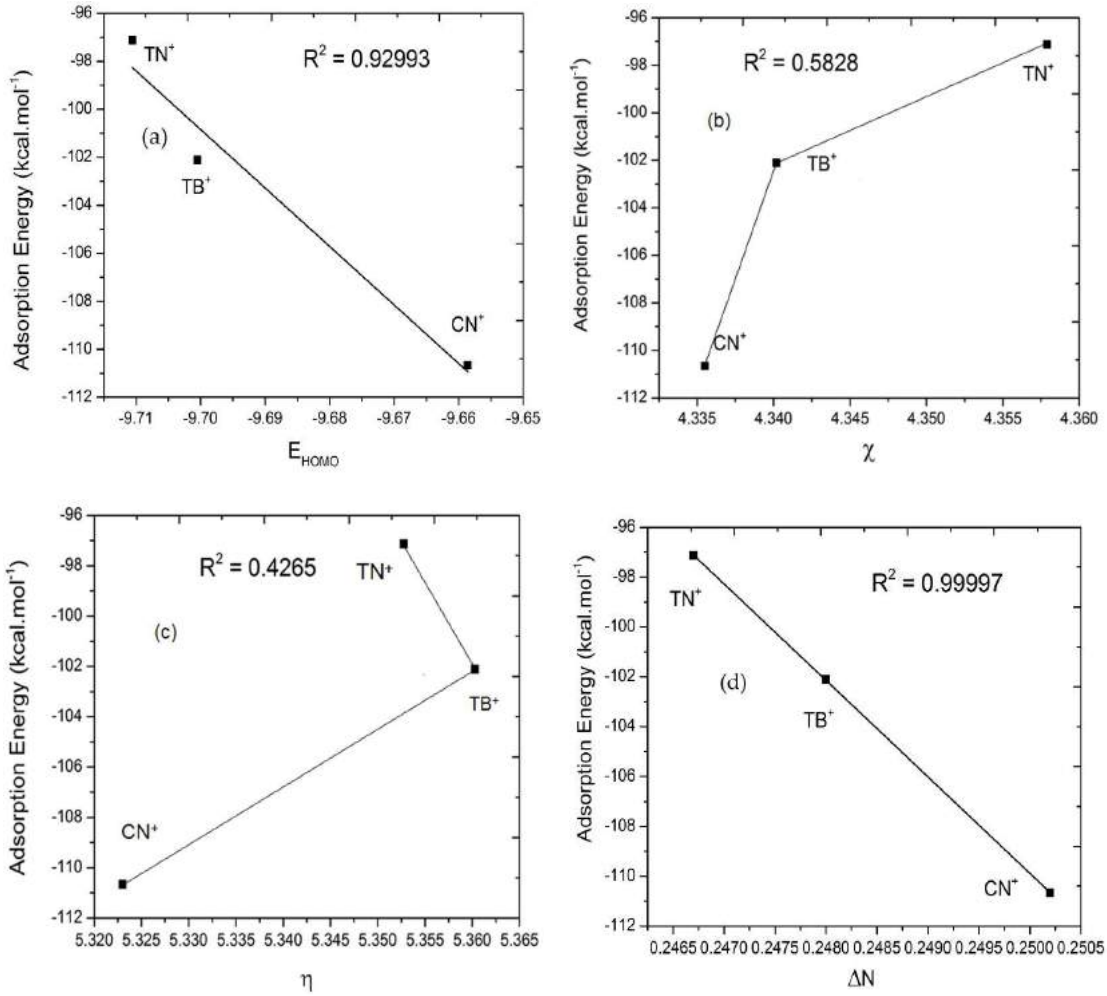

Figure 6. Correlation of the adsorption energy and quantum parameters such as EHOMO, electronegativity, hardness, and electron transfer of protonated inhibitors (caffeine (CN^+), theophylline (TP^+), and theobromine (TB^+)) in copper surface. (**a**) The correlation between the adsorption energy and EHOMO, (**b**) the adsorption energy and electronegativity, (**c**) the adsorption energy and hardness, (**d**) the adsorption energy and electron transfer.

4. Conclusions

This theoretical study aims to evaluate caffeine, theobromine, and theophylline's corrosion inhibition performance against copper corrosion in gas and aqueous conditions. The density functional theory at B3LYP function and ab initio MP2 at various levels of theory and Monte Carlo simulation study were employed to evaluate the corrosion inhibition efficiency and to provide a detailed picture of the mechanism of corrosion inhibition of these three compounds on the copper surface. According to all data given in this study, caffeine, theobromine, and theophylline will be effective in preventing the corrosion of copper. The DFT, MP2 approach, and Monte Carlo simulation study showed that the inhibition efficiency ranking of studied molecules in preventing corrosion of copper as caffeine > theobromine > theophylline. The adsorption energy obtained in the study shows that the most effective inhibitor among them is caffeine. The theoretical research agrees with the results of previously published experimental studies by de Souza et al. This theoretical study will help the rational design of a more effective caffeine-based corrosion inhibitor.

Author Contributions: Conceptualization, S.H. (Saprizal Hadisaputra) and A.A.P.; methodology, N.P. and S.H. (Saprizal Hadisaputra); data curation, E.Y., S.H. (Saprini Hamdiani); writing—original draft preparation, S.H. (Saprizal Hadisaputra), N.P., and E.Y.; writing—review and editing, L.R.T.S., A.A.P., and S.H. (Saprizal Hadisaputra). All authors have read and agreed to the published version of the manuscript.

Funding: This research was funded by Kemenristekdikti Republic of Indonesia, Grant No. 1730/UN18.L1/PP/2020 and The APC was funded by Kemenristekdikti Republic of Indonesia, Grant No. 1730/UN18.L1/PP/2020.

Acknowledgments: Financially supported by Kemenristekdikti Republic of Indonesia through Penelitian Dasar 2020, Grant No. 1730/UN18.L1/PP/2020, is gratefully acknowledged.

Conflicts of Interest: The authors declare no conflict of interest.

References

1. Umoren, S.A.; Solomon, M.M.; Obot, I.B.; Sulieman, R.K. A critical review on the recent studies on plant biomaterials as corrosion inhibitors for industrial metals. *J. Ind. Eng. Chem.* **2019**, *76*, 91–115. [CrossRef]
2. Xhanari, K.; Finšgar, M.; Hrnčič, M.K.; Maver, U.; Knez, Ž.; Seiti, B. Green corrosion inhibitors for aluminium and its alloys: A review. *RSC Adv.* **2017**, *7*, 27299–27330. [CrossRef]
3. Hadisaputra, S.; Purwoko, A.A.; Rahmawati; Asnawati, D.; Hamdiani, I.S.; Nuryono. Experimental and Theoretical Studies of (2R)-5-hydroxy-7-methoxy-2-phenyl-2, 3-dihydrochromen-4-one as corrosion inhibitor for Iron in Hydrochloric Acid. *Int. J. Electrochem. Sci.* **2019**, *14*, 11110–11121. [CrossRef]
4. Sedik, A.; Lerari, D.; Salci, A.; Athmani, S.; Bachari, K.; Gecibesler, İ.H.; Solmaz, R. Dardagan Fruit extract as eco-friendly corrosion inhibitor for mild steel in 1 M HCl: Electrochemical and surface morphological studies. *J. Taiwan Inst. Chem. Eng.* **2020**, *107*, 189–200. [CrossRef]
5. Hadisaputra, S.; Purwoko, A.A.; Ilhamsyah, I.; Hamdiani, S.; Suhendra, D.; Nuryono, N.; Bundjali, B. A combined experimental and theoretical study of (E)-ethyl 3-(4-methoxyphenyl) acrylate as corrosion inhibitor of iron in 1 M HCl solutions. *Int. J. Corros. Scale Inhib.* **2018**, *7*, 633–647. [CrossRef]
6. Vu, N.S.H.; Binh, P.M.Q.; Ai, D.V.; Thu, V.T.H.; van Hien, P.; Panaitescu, C.; Nam, N.D. Combined experimental and computational studies on corrosion inhibition of Houttuynia cordata leaf extract for steel in HCl medium. *J. Mol. Liq.* **2020**, 113787. [CrossRef]
7. Verma, D.K.; Al Fantazi, A.; Verma, C.; Khan, F.; Asatkar, A.; Hussain, C.M.; Ebenso, E.E. Experimental and computational studies on hydroxamic acids as environmental friendly chelating corrosion inhibitors for mild steel in aqueous acidic medium. *J. Mol. Liq.* **2020**, 113651. [CrossRef]
8. Faiz, M.; Zahari, A.; Awang, K.; Hussin, H. Corrosion inhibition on mild steel in 1 M HCl solution by Cryptocarya nigra extracts and three of its constituents (alkaloids). *RSC Adv.* **2002**, *10*, 6547–6562. [CrossRef]
9. Ngouné, B.; Pengou, M.; Nanseu-Njiki, C.P.; Ngameni, E. A comparative study using solution analysis, electrochemistry and mass change for the inhibition of carbon steel by the plant alkaloid Voacangine. *Corros. Eng. Sci. Technol.* **2020**, *55*, 138–144. [CrossRef]
10. Thomas, A.; Prajila, M.; Shainy, K.M.; Joseph, A. A green approach to corrosion inhibition of mild steel in hydrochloric acid using fruit rind extract of Garcinia indica (Binda). *J. Mol. Liq.* **2020**, 113369. [CrossRef]
11. Umoren, S.A.; Solomon, M.M.; Madhankumar, A.; Obot, I.B. Exploration of natural polymers for use as green corrosion inhibitors for AZ31 magnesium alloy in saline environment. *Carbohydr. Polym.* **2020**, *230*, 115466. [CrossRef]
12. Dutta, A.; Saha, S.K.; Adhikari, U.; Banerjee, P.; Sukul, D. Effect of substitution on corrosion inhibition properties of 2-(substituted phenyl) benzimidazole derivatives on mild steel in 1 M HCl solution: A combined experimental and theoretical approach. *Corros. Sci.* **2017**, *123*, 256–266. [CrossRef]
13. Hamidon, T.S.; Hussin, M.H. Susceptibility of hybrid sol-gel (TEOS-APTES) doped with caffeine as potent corrosion protective coatings for mild steel in 3.5 wt.% NaCl. *Prog. Org. Coat.* **2020**, *140*, 105478. [CrossRef]
14. Espinoza-Vázquez, A.; Rodríguez-Gómez, F.J. Caffeine and nicotine in 3% NaCl solution with CO_2 as corrosion inhibitors for low carbon steel. *RSC Adv.* **2016**, *6*, 70226–70236. [CrossRef]
15. Gudić, S.; Oguzie, E.E.; Radonić, A.; Vrsalović, L.; Smoljko, I.; Kliškić, M. Inhibition of copper corrosion in chloride solution by caffeine isolated from black tea. *Maced. J. Chem. Chem. Eng.* **2014**, *33*, 13–25. [CrossRef]
16. Fallavena, T.; Antonow, M.; Gonçalves, R.S. Caffeine as non-toxic corrosion inhibitor for copper in aqueous solutions of potassium nitrate. *Appl. Surf. Sci.* **2006**, *253*, 566–571. [CrossRef]

17. Rajendran, S.; Amalraj, A.J.; Joice, M.J.; Anthony, N.; Trivedi, D.C.; Sundaravadivelu, M. Corrosion inhibition by the caffeine-Zn^{2+} system. *Corros. Rev.* **2004**, *22*, 233–248. [CrossRef]
18. da Trindade, L.G.; Goncalves, R.S. Evidence of caffeine adsorption on a low-carbon steel surface in ethanol. *Corros. Sci.* **2009**, *51*, 1578–1583. [CrossRef]
19. Ebadi, M.; Basirun, W.J.; Leng, S.Y.; Mahmoudian, M.R. Investigation of corrosion inhibition properties of caffeine on nickel by electrochemical techniques. *Int. J. Electrochem. Sci.* **2012**, *7*, 8052–8063.
20. de Souza, F.S.; Giacomelli, C.; Gonçalves, R.S.; Spinelli, A. Adsorption behavior of caffeine as a green corrosion inhibitor for copper. *Mater. Sci. Eng. C* **2012**, *32*, 2436–2444. [CrossRef]
21. Ammouchi, N.; Allal, H.; Belhocine, Y.; Bettaz, S.; Zouaoui, E. DFT computations and molecular dynamics investigations on conformers of some pyrazinamide derivatives as corrosion inhibitors for aluminum. *J. Mol. Liq.* **2020**, *300*, 112309. [CrossRef]
22. Hadisaputra, S.; Purwoko, A.A.; Wajdi, F.; Sumarlan, I.; Hamdiani, S. Theoretical study of the substituent effect on corrosion inhibition performance of benzimidazole and its derivatives. *Int. J. Corros. Scale Inhib.* **2019**, *8*, 673–688. [CrossRef]
23. Obot, I.B.; Macdonald, D.D.; Gasem, Z.M. Density functional theory (DFT) as a powerful tool for designing new organic corrosion inhibitors. Part 1: An overview. *Corros. Sci.* **2015**, *99*, 1–30. [CrossRef]
24. Hadisaputra, S.; Hamdiani, S.; Kurniawan, M.A.; Nuryono, N. Influence of macrocyclic ring size on the corrosion inhibition efficiency of dibenzo crown ether: A density functional study. *Indones. J. Chem.* **2017**, *17*, 431–438. [CrossRef]
25. Hsissou, R.; Benhiba, F.; Abbout, S.; Dagdag, O.; Benkhaya, S.; Berisha, A.; Elharfi, A. Trifunctional epoxy polymer as corrosion inhibition material for carbon steel in 1.0 M HCl: MD simulations, DFT and complexation computations. *Inorg. Chem. Commun.* **2020**, 107858. [CrossRef]
26. Hadisaputra, S.; Purwoko, A.A.; Hakim, A.; Savalas, L.R.T.; Rahmawati, R.; Hamdiani, S.; Nuryono, N. Ab initio MP2 and DFT studies of ethyl-p-methoxycinnamate and its derivatives as corrosion inhibitors of iron in acidic medium. *J. Phys. Conf. Ser.* **2019**, *1402*, 055046. [CrossRef]
27. Karakus, N.; Sayin, K. The investigation of corrosion inhibition efficiency on some benzaldehyde thiosemicarbazones and their thiole tautomers: Computational study. *J. Taiwan Inst. Chem. Eng.* **2015**, *48*, 95–102. [CrossRef]
28. El Ibrahimi, B.; Jmiai, A.; Bazzi, L.; El Issami, S. Amino acids and their derivatives as corrosion inhibitors for metals and alloys. *Arab J. Chem.* **2020**, *13*, 740–771. [CrossRef]
29. Sasikumar, Y.; Adekunle, A.S.; Olasunkanmi, L.O.; Bahadur, I.; Baskar, R.; Kabanda, M.M.; Ebenso, E.E. Experimental, quantum chemical and Monte Carlo simulation studies on the corrosion inhibition of some alkyl imidazolium ionic liquids containing tetrafluoroborate anion on mild steel in acidic medium. *J. Mol. Liq.* **2015**, *211*, 105–118. [CrossRef]
30. Obot, I.B.; Haruna, K.; Saleh, T.A. Atomistic Simulation: A Unique and Powerful Computational Tool for Corrosion Inhibition Research. *Arab J. Sci. Eng.* **2019**, *44*, 1–32. [CrossRef]
31. Kaya, S.; Kaya, C.; Guo, L.; Kandemirli, F.; Tüzün, B.; Uğurlu, İ.; Saraçoğlu, M. Quantum chemical and molecular dynamics simulation studies on inhibition performances of some thiazole and thiadiazole derivatives against corrosion of iron. *J. Mol. Liq.* **2016**, *219*, 497–504. [CrossRef]
32. Kaya, S.; Guo, L.; Kaya, C.; Tüzün, B.; Obot, I.B.; Touir, R.; Islam, N. Quantum chemical and molecular dynamic simulation studies for the prediction of inhibition efficiencies of some piperidine derivatives on the corrosion of iron. *J. Taiwan Inst. Chem. Eng.* **2016**, *65*, 522–529. [CrossRef]
33. Adamo, C.; Jacquemin, D. The calculations of excited-state properties with Time-Dependent Density Functional Theory. *Chem. Soc. Rev.* **2013**, *42*, 845–856. [CrossRef] [PubMed]
34. Harding, L.B.; Klippenstein, S.J.; Jasper, A.W. Ab initio methods for reactive potential surfaces. *Phys. Chem. Chem. Phys.* **2017**, *9*, 4055–4070. [CrossRef]
35. Frisch, M.J.; Trucks, G.W.; Schlegel, H.B.; Scuseria, G.E.; Robb, M.A.; Cheeseman, J.R.; Scalmani, G. *No. 3 Gaussian*; Revision 02; Gaussian09, Inc.: Wallingford, UK, 2009; p. 4.
36. Hadisaputra, S.; Canaval, L.R.; Pranowo, H.D.; Armunanto, R. Theoretical study of substituent effects on Cs^{+}/Sr^{2+}–dibenzo-18-crown-6 complexes. *Monat. Chem.* **2014**, *145*, 737–745. [CrossRef]
37. Varadwaj, P.R.; Varadwaj, A.; Marques, H.M. DFT-B3LYP, NPA-, and QTAIM-based study of the physical properties of [M (II)$(H_2O)_2$(15-crown-5)](M=Mn, Fe, Co, Ni, Cu, Zn) complexes. *J. Phys. Chem. A* **2011**, *115*, 5592–5601. [CrossRef]

38. Koopmans, T. Über ydie zuordnung von wellenfunktionen und eigenwerten zu den einzelnen elektronen eines atoms. *Physica* **1934**, *1*, 104–113. [CrossRef]
39. Islam, N.; Chandra Ghosh, D. A new algorithm for the evaluation of the global hardness of polyatomic molecules. *Mol. Phys.* **2011**, *109*, 917–931. [CrossRef]
40. Parr, R.G.; Szentpaly, L.V.; Liu, S. Electrophilicity index. *J. Am. Chem. Soc.* **1999**, *121*, 1922–1924. [CrossRef]
41. Yang, W.; Parr, R.G. Hardness, softness, and the fukui function in the electronic theory of metals and catalysis. *Proc. Natl. Acad. Sci. USA* **1985**, *82*, 6723–6726. [CrossRef]
42. Pearson, R.G. Hard and soft acids and bases—the evolution of a chemical concept. *Coord. Chem. Rev.* **1990**, *100*, 403–425. [CrossRef]
43. Pearson, R.G. Absolute electronegativity and hardness: Application to inorganic chemistry. *Inorg. Chem.* **1988**, *27*, 734–740. [CrossRef]
44. Sastri, V.S.; Perumareddi, J.R. Molecular orbital theoretical studies of some organic corrosion inhibitors. *Corros. Sci.* **1997**, *53*, 617–622. [CrossRef]
45. Obot, I.B.; Gasem, Z.M. Theoretical evaluation of corrosion inhibition performance of some pyrazine derivatives. *Corros. Sci.* **2014**, *83*, 359–366. [CrossRef]
46. Khaled, K.F. Monte Carlo simulations of corrosion inhibition of mild steel in 0.5 M sulphuric acid by some green corrosion inhibitors. *J. Solid State Electrochem.* **2009**, *13*, 1743–1756. [CrossRef]
47. Khaled, K.F.; El-Maghraby, A. Experimental, Monte Carlo and molecular dynamics simulations to investigate corrosion inhibition of mild steel in hydrochloric acid solutions. *Arab. J. Chem.* **2014**, *7*, 319–326. [CrossRef]
48. Frenkel, D.; Smit, B. *Understanding Molecular Simulations: From Algorithms to Applications*, 2nd ed.; Academic Press: San Diego, CA, USA, 2002.
49. Kirkpatrick, S.; Gelatt, C.D.; Vecchi, M.P. Optimization by simulated annealing. *Science* **1983**, *220*, 671–680. [CrossRef]
50. Madkour, L.H.; Kaya, S.; Obot, I.B. Computational, Monte Carlo simulation and experimental studies of some arylazotriazoles (AATR) and their copper complexes in corrosion inhibition process. *J. Mol. Liq.* **2018**, *260*, 351–374. [CrossRef]
51. Tang, J.; Qiu, R.; Chen, J.; Ao, B. Diffusion behavior of hydrogen in oxygen saturated and unsaturated plutonium dioxide: An ab initio molecular dynamics study. *J. Alloys Compd.* **2020**, *834*, 155113. [CrossRef]
52. Sutor, D.J. The structures of the pyrimidines and purines. VII. The crystal structure of caffeine. *Acta Cryst.* **1958**, *11*, 453–458. [CrossRef]
53. Ford, K.A.; Ebisuzaki, Y.; Boyle, P.D. Methylxanthines. II. Anhydrous Theobromine. *Acta Cryst. Sec. C Cryst. Struct. Commun.* **1998**, *54*, 1980–1983. [CrossRef]
54. Ebisuzaki, Y.; Boyle, P.D.; Smith, J.A. Methylxanthines. i. anhydrous theophylline. *Acta Cryst. Sec. C Cryst. Struct. Commun.* **1997**, *53*, 777–779. [CrossRef]
55. Feyer, V.; Plekan, O.; Richter, R.; Coreno, M.; Prince, K.C. Photoion mass spectroscopy and valence photoionization of hypoxanthine, xanthine and caffeine. *Chem. Phys.* **2019**, *358*, 3–38. [CrossRef]
56. Ajò, D.; Cingi, M.B.; Fragalá, I.; Granozzi, G. UV Phoelectron Spectra of Biological Xanthines: Theophylline, Theobromine and Caffeine. *Spectrosc. Lett.* **1977**, *10*, 757–761. [CrossRef]
57. Hadisaputra, S.; Purwoko, A.A.; Wirayani, Y.; Ulfa, M.; Hamdiani, S. Density functional and perturbation calculation on the corrosion inhibition performance of benzylnicotine and its derivatives. *AIP Conf. Proc.* **2020**, *243*, 020006. [CrossRef]
58. Dobeš, P.; Otyepka, M.; Strnad, M.; Hobza, P. Interaction Energies for the Purine Inhibitor Roscovitine with Cyclin-Dependent Kinase 2: Correlated Ab Initio Quantum-Chemical, DFT and Empirical Calculations. *Chem. Euro. J.* **2006**, *12*, 4297–4304. [CrossRef]
59. Reimers, J.R.; Cai, Z.L.; Bilić, A.; Hush, N.S. The Appropriateness of Density-Functional Theory for the Calculation of Molecular Electronics Properties. *Ann. N. Y. Acad. Sci.* **2003**, *1006*, 235–251. [CrossRef]
60. Kokalj, A.; Kovačević, N. On the consistent use of electrophilicity index and HSAB-based electron transfer and its associated change of energy parameters. *Chem. Phys. Lett.* **2011**, *507*, 181–184. [CrossRef]
61. Siaka, A.A.; Eddy, N.O.; Idris, S.; Magaji, L. Experimental and computational study of corrosion potentials of penicillin G. *Res. J. Appl. Sci.* **2011**, *6*, 487–493. [CrossRef]
62. Eddy, N.O.; Stoyanov, S.R.; Ebenso, E.E. Fluoroquinolones as corrosion inhibitors for mild steel in acidic medium; experimental and theoretical studies. *Int. J. Electrochem. Sci.* **2010**, *5*, 1127–1150.

63. Shi, W.; Xia, M.; Lei, W.; Wang, F. Molecular dynamics study of polyether polyamino methylene phosphonates as an inhibitor of anhydrite crystal. *Desalination* **2013**, *322*, 137–143. [CrossRef]
64. Umoren, S.A.; Obot, I.B.; Madhankumar, A.; Gasem, Z.M. Effect of degree of hydrolysis of polyvinyl alcohol on the corrosion inhibition of steel: Theoretical and experimental studies. *J. Adhe. Sci. Tech.* **2015**, *29*, 271–295. [CrossRef]